Reprinted from The Journal of Physical Chemistry, 1995, 99.

Theoretical Study of the Vacuum-Ultraviolet Spectra of SnH_4 and $Sn(CH_3)_4$

Koji Yasuda,† Naoki Kishimoto, and Hiroshi Nakatsuji*,‡

Department of Synthetic Chemistry and Biological Chemistry, Faculty of Engineering, Kyoto University, Kyoto 606, Japan

Received: January 6, 1995; In Final Form: May 24, 1995⊗

The excitation spectra of SnH_4 and $Sn(CH_3)_4$ were studied theoretically by the SAC-CI (symmetry adapted cluster–configuration interaction) method. The calculated spectra agree well with the observed vacuum-ultraviolet (VUV) spectra. The results of the lowest states agree with the earlier works by Fernandez et al. In higher energy region, the earlier works have overlooked many states which constitute broad observed bands. The new assignments of the spectra up to the first ionization potential are given, and the natures of the excitations are discussed. The excitations in this energy region are primarily Rydberg in nature, though some states show a strong mixing with the valence antibonding states. The difference in the VUV spectra between SnH_4 and $Sn(CH_3)_4$ is attributed to the difference in the nodes of the $t_2\sigma^*$ antibonding orbitals.

Introduction

Stannanes, together with silanes and germanes, are now widely used in electronic devices.[1,2] Their excited-state properties play a central role in the initial step of chemical vapor deposition processes.[1,2] Photochemical reactions of stannanes are also of interest with regard to the pollution of sea water.[3] Though some studies have examined the photochemistry of methane and silanes,[2,4] there are few experimental or theoretical studies of stannanes.

Fernandez et al. recorded the vacuum-ultraviolet (VUV) spectra of some stannanes and compared them with the results of ab initio calculations,[5,6] which are shown in the insets of Figures 1 and 2. As shown, their assignments seem to be reliable for the lower excited states but less reliable for higher excited states, especially for $Sn(CH_3)_4$. In addition, no Rydberg series were calculated, which must exist in this energy region.

It is generally recognized that most transitions of saturated hydrocarbon analogues are Rydberg-type excitations,[7] some of which mix with valence antibonding states. This mixing strongly changes the nature of the Rydberg excitations.[7,8] Since the antibonding orbitals of stannanes are lower than those of hydrocarbon analogues, Rydberg/valence mixing becomes more important. We were also interested in the difference in mixing due to the symmetry difference of various antibonding orbitals. We can examine this Rydberg/valence mixing by ab initio calculations with large basis sets including Rydberg functions.

In this study, we investigated the excited states of SnH_4 and $Sn(CH_3)_4$ to explain the VUV spectra and the nature of the excited states below the first ionization potential (IP). We used the symmetry adapted cluster (SAC)[9]/symmetry adapted cluster–configuration interaction (SAC-CI) method,[10] which has been applied to many molecules, including transition metal complexes.[11,12] We have shown that this method is very useful for investigating excited states over a wide energy range and has yielded many reliable assignments of experimental spectra. A review is given in ref 11.

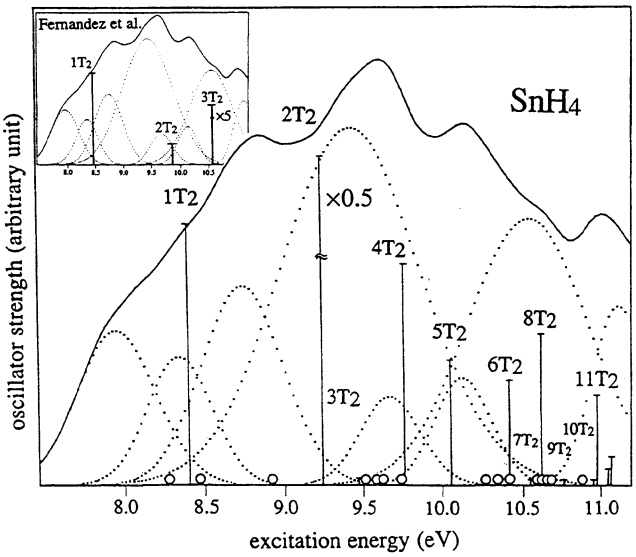

Figure 1. SAC-CI theoretical excitation spectrum of SnH_4 below the first IP, 11.27 eV, compared with the observed spectrum (ref 5). Inset is the spectrum calculated by Fernandez et al. (ref 5).

Method for the Calculations

We used the experimental bond lengths and angles in the vapor phase:[13] for SnH_4, Sn–H = 1.7108 Å, ∠HSnH = 109.47°; for $Sn(CH_3)_4$, Sn–C = 2.144 Å, C–H = 1.118 Å, ∠SnCH = 112.0°, ∠CSnC = 109.47°. We assumed T_d symmetry for $Sn(CH_3)_4$. Effective core potentials (ECPs) are often used to account for relativistic effects with heavy atoms. However, since some ECPs yield poor results for excited states,[12b] we used all-electron basis sets. We used Cartesian Gaussian functions in this calculation: for SnH_4, Huzinaga's Sn(16s13p7d)/[7s6p2d] set[14] with two d-type polarization functions (ζ_d = 0.253, 0.078)[14] and Dunning's H(4s)/[3s] set;[15] for $Sn(CH_3)_4$, Huzinaga's Sn(16s13p7d)/[7s6p2d] set[14] with one d-type polarization function (ζ_d = 0.183),[14] Dunning's C(9s5p)/[3s2p] set,[15] and Huzinaga's H(4s)/[1s] set.[14] Since Rydberg-type excitations are expected to be important, several Rydberg functions determined by Jungen's method[16] were added, as shown in Table 1. For SnH_4, we added five s, p, and d Gaussian functions on Sn and two s and p functions on each hydrogen. Since the overlap between the most diffuse functions on Sn and H is nearly unity, no additional diffuse functions are needed on

* To whom correspondence should be addressed.
† Research Fellow of the Japan Society for the Promotion of Science for Young Scientists.
‡ Also affiliated with the Institute for Fundamental Chemistry, 34-4, Takano-Nishihikari-cho, Sakyo-ku, Kyoto 606, Japan.
⊗ Abstract published in *Advance ACS Abstracts,* July 15, 1995.

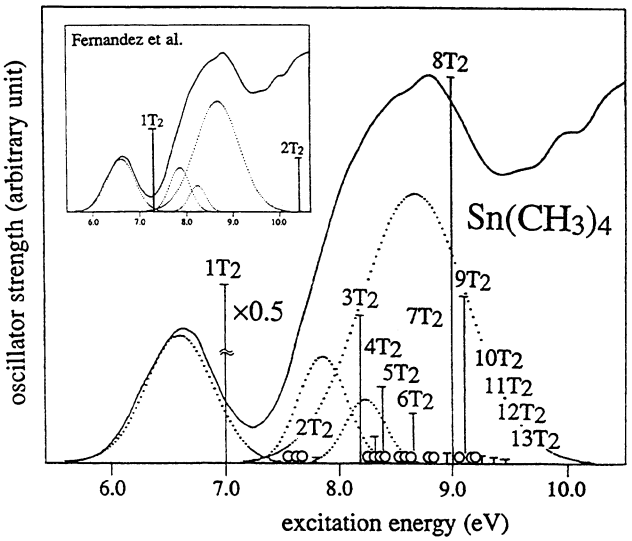

Figure 2. SAC-CI theoretical excitation spectrum of $Sn(CH_3)_4$ below the first IP, 9.70 eV, compared with the observed spectrum (ref 6). Inset is the spectrum calculated by Fernandez et al. (ref 6).

TABLE 1: Diffuse Cartesian Gaussian Functions Used in the Calculations

Gaussian type	exponents
	SnH_4
on Sn	
s type	0.025 71, 0.010 94, 0.005 414, 0.002 977, 0.001 769
p type	0.017 87, 0.008 135, 0.004 216, 0.002 398, 0.001 463
d type	0.025 71, 0.010 94, 0.005 414, 0.002 977, 0.001 769
on hydrogen	
s type	0.047 63, 0.017 87
p type	0.047 63, 0.008 135
	$Sn(CH_3)_4$
on Sn	
s type	0.021 34, 0.009 408, 0.004 768
p type	0.015 07, 0.007 069, 0.003 742
d type	0.047 63, 0.017 87, 0.008 135
on carbon	
s type	0.023
p type	0.021

hydrogens. For $Sn(CH_3)_4$, we added three s, p, and d Gaussian functions on Sn and one s and p function on each carbon, which were taken from ref 17.

For SnH_4, the total number of atomic orbitals is 153, while the total number of molecular orbitals is 142. For $Sn(CH_3)_4$, these are 133 and 131, respectively. Since our basis sets involve very diffuse functions, none of them are linearly independent: we eliminated the subspace of the basis set which is linearly dependent to the others.

The ground-state electron correlations were calculated by the SAC method,[9] while the excited states were calculated by the SAC-CI method.[10] The Hartree–Fock (HF) MOs were used as reference orbitals. We used the SAC85 program[18] in this calculation.

The active space in the SAC/SAC-CI calculation consists of 4 occupied and 100 unoccupied orbitals for SnH_4 and 16 occupied and 82 unoccupied orbitals for $Sn(CH_3)_4$. This includes all of the occupied valence MOs. All of the single-excitation operators were included, while the double-excitation operators were selected by the second-order perturbation method.[19] In the present calculation, we used the following thresholds: 1.0×10^{-5} au for the ground, excited, and ionized states of SnH_4, 4.0×10^{-5} au for the ground state of $Sn(CH_3)_4$, and 8.0×10^{-5} au for the excited states of $Sn(CH_3)_4$. The SAC85 program includes some triple and quadruple excitations

TABLE 2: Energies and Nature of Hartree–Fock Valence Occupied Orbitals of SnH_4 and $Sn(CH_3)_4$

symmetry	orbital energy (eV)	orbital nature[a]
	SnH_4	
$5a_1$	−17.96	Sn(5s) + H(s)
$6t_2$	−12.28	Sn(5p) + H(s); HOMO
	$Sn(CH_3)_4$	
$6a_1$	−25.48	C(s) + H(s)
$7t_2$	−24.66	C(s) + H(s)
$7a_1$	−15.70	Sn(5s) + C(p)
$8t_2$	−14.85	C(p) + H(s)
3e	−14.77	C(p) + H(s)
$1t_1$	−14.25	C(p) + H(s)
$9t_2$	−10.76	Sn(5p) + C(p); HOMO

[a] + indicates a bonding combination.

which are the products of the lower excitation operators.[19] The dimensions of the present calculations are about 1600–2600 for the ground states, 8600–9600 for the excited states, and 400–470 for the ionized states.

Results for SnH_4

Ground State. The energies and the nature of the HF valence occupied MOs of SnH_4 are shown in Table 2, in which + denotes a bonding combination. The $5a_1$ MO is the Sn(5s)+H(s) bonding MO, while the highest occupied MOs (HOMOs) $6t_2$ are the Sn(5p)+H(s) bonding MOs. These four bonding MOs represent the four Sn–H bonds. There are many unoccupied MOs with small positive orbital energies, which mainly consist of diffuse basis functions. They are electron-accepting orbitals of neutral SnH_4, rather than bounded Rydberg orbitals.

The Hartree–Fock total energy of SnH_4 is −6020.8211 au, and the correlation energy calculated by the SAC method is −0.077 23 au, which represents 12 kcal/mol per bond.

Comparison with the VUV Spectrum of SnH_4. Figure 1 compares our SAC-CI results with the experimental spectrum of SnH_4. The dotted peaks show the result of the deconvolution analysis by Fernandez et al.[5] Table 3 gives the details of the calculated T_2 states. The T_2 states are the only optically allowed states in the T_d symmetry. The optically forbidden transitions are shown in Figure 1 by open circles on the energy axis; details are given in Table 4.

The inset of Figure 1 shows the result of ab initio calculations by Fernandez et al. Though they gave only three T_2 states in this energy region, our results show many T_2 states. For example, the strongest absorption at 9.7 eV is not explained by their result. For studying the excited states of saturated molecules like SnH_4, it is essential to include not only the valence-type basis functions but also many Rydberg-type basis functions. Since Fernandez et al. did not include enough Rydberg-type functions, their result is unreliable except for the lowest state.

The first broad absorption centered at 8.7 eV appears as a shoulder of the absorption spectrum. We calculated the $1T_2$ state at 8.40 eV, which reflects a mixed Rydberg 6s and $a_1\sigma^*$ antibonding nature. Fernandez et al. analyzed this band as a superposition of three peaks separated by 0.4 eV and concluded that they showed Jahn–Teller splitting.[5] The first band of the photoelectron spectrum shows a similar Jahn–Teller splitting.[20] Since this T_2 state shows a mixture of Rydberg and antibonding orbitals, and since no other T_2 states were calculated in this region, we also interpreted these three peaks in the deconvolution analysis as Jahn–Teller splitting.

The second broad absorption is centered at 9.7 eV, while the deconvolution analysis shows a strong peak at 9.4 eV and a weak peak at 9.7 eV. We considered this band to be a

TABLE 3: Excitation Energies, Oscillator Strengths, and the Nature of the Singlet T_2 (Dipole-Allowed) Excited States of SnH_4

				Mulliken population[a]							
				Sn					H		
state	excitation energy (eV)	oscillator strength ($\times 10^{-2}$)	second moment (au)	val s	val p	Ryd s	Ryd p	Ryd d	val s	Ryd s	nature[b]
XA_1	0.0		112	0.86	1.24	−0.03	0.31	−0.01	1.05	0.33	ground state, Hartree−Fock
$1T_2$	8.40	45.8	155	0.69	1.51	0.21	0.36	0.03	0.91	0.31	Sn(p)+H(s) → Sn(6s), Sn(5s)−H(s)
$2T_2$	9.24	117	146	0.79	1.74	−0.02	0.41	0.27	0.91	0.17	Sn(p)+H(s) → Sn(5d), Sn(5p)−H(s)
$3T_2$	9.47	0.82	204	0.77	1.38	0.00	1.01	0.13	0.90	0.23	Sn(p)+H(s) → Sn(6p)
$4T_2$	9.77	37.6	192	0.77	1.51	−0.02	0.33	0.63	0.91	0.16	Sn(p)+H(s) → Sn(5d), Sn(5p)−H(s)
$5T_2$	10.07	21.8	333	0.76	1.59	0.33	0.29	0.63	0.91	0.15	Sn(p)+H(s) → Sn(7s)
$6T_2$	10.41	17.8	378	0.81	1.62	−0.03	0.34	0.83	0.90	0.11	Sn(p)+H(s) → Sn(6d)
$7T_2$	10.55	0.05	563	0.77	1.50	−0.01	0.99	0.27	0.90	0.15	Sn(p)+H(s) → Sn(7p)
$8T_2$	10.64	26.2	583	0.80	1.61	0.04	0.34	0.83	0.91	0.13	Sn(p)+H(s) → Sn(6d)
$9T_2$	10.78	0.22	611	0.86	1.61	−0.06	0.33	0.64	0.90	0.05	Sn(p)+H(s) → Sn(8s)
$10T_2$	10.97	0.72	1332	0.78	1.69	−0.04	0.32	0.82	0.90	0.09	Sn(p)+H(s) → Sn(8p)
$11T_2$	10.99	15.9	923	0.77	1.70	−0.01	0.30	1.17	0.90	0.11	Sn(p)+H(s) → Sn(7d)

[a] Abbreviations: val and Ryd = valence and Rydberg, respectively. [b] + and − indicate bonding and antibonding combinations.

TABLE 4: Excitation Energies and the Nature of the Singlet A_1, E, and T_1 (Dipole-Forbidden) Excited States of SnH_4

			Mulliken population[a]							
			Sn					H		
state	excitation energy (eV)	second moment (au)	val s	val p	Ryd s	Ryd p	Ryd d	val s	Ryd s	nature[b]
XA_1	0.0	110	0.86	1.24	−0.03	0.31	−0.01	1.05	0.33	ground state, Hartree−Fock
$1T_1$	8.27	128	0.76	1.68	−0.02	0.34	0.08	0.94	0.17	Sn(p)+H(s) → Sn(5p)−H(s)
1E	8.48	131	0.78	1.45	−0.02	0.43	0.13	0.95	0.21	Sn(p)+H(s) → Sn(5p)−H(s)
$1A_1$	8.92	137	0.77	1.55	−0.02	0.61	0.07	0.92	0.20	Sn(p)+H(s) → Sn(5p)−H(s)
$2A_1$	9.48	213	0.76	1.54	−0.02	0.83	0.07	0.90	0.18	Sn(p)+H(s) → Sn(6p)
$2T_1$	9.59	204	0.76	1.49	−0.02	0.76	0.29	0.90	0.18	Sn(p)+H(s) → Sn(6p)
2E	9.61	212	0.79	1.44	−0.02	1.09	0.09	0.90	0.21	Sn(p)+H(s) → Sn(6p)
$3T_1$	9.75	192	0.76	1.48	−0.02	0.78	0.41	0.89	0.19	Sn(p)+H(s) → Sn(7p)
$4T_1$	10.27	333	0.78	1.65	−0.02	0.31	1.12	0.90	0.11	Sn(p)+H(s) → Sn(5d)
3E	10.35	356	0.78	1.66	−0.02	0.39	1.00	0.90	0.11	Sn(p)+H(s) → Sn(5d)
$3A_1$	10.42	450	0.78	1.56	−0.02	0.98	0.24	0.90	0.13	Sn(p)+H(s) → Sn(7p)
$5T_1$	10.55	505	0.77	1.54	−0.02	0.53	0.72	0.90	0.15	Sn(p)+H(s) → Sn(5d)
$4A_1$	10.57	460	0.78	1.56	−0.02	0.66	0.68	0.90	0.14	Sn(p)+H(s) → Sn(5d)
4E	10.57	601	0.77	1.57	−0.02	1.11	0.11	0.89	0.14	Sn(p)+H(s) → Sn(7p)
$6T_1$	10.59	598	0.78	1.55	−0.02	0.95	0.26	0.90	0.14	Sn(p)+H(s) → Sn(8p)
$7T_1$	10.88	750	0.78	1.73	−0.02	0.26	1.26	0.90	0.07	Sn(p)+H(s) → Sn(6d)

[a] Abbrevations: val and Ryd = valence and Rydberg, respectively. [b] + and − indicate bonding and antibonding combinations.

superposition of two states: $2T_2$ calculated at 9.24 eV and $4T_2$ at 9.77 eV. These represent the Rydberg 5d mixed with the $t_2\sigma^*$ antibonding orbitals. As seen in Table 3, the $2T_2$ state has the largest calculated oscillator strength, which implies that it has a stronger antibonding nature than the $4T_2$ state. Note that the $3T_2$ state calculated at 9.47 eV has a very small oscillator strength.

The ab initio calculation by Fernandez et al. showed that this peak has a Rydberg p character. However, their calculated Rydberg p state has a much smaller oscillator strength than the experimental value. Since they did not include diffuse d functions, they might have overlooked this Rydberg d state.

In the higher energy region, the spectrum shows several bands centered at 10.2, 10.7, and 11.1 eV, while the deconvolution analysis shows peaks at 10.2, 10.6, and 11.2 eV. We obtained many states in this energy region. Among them, $5T_2$, $6T_2$, $8T_2$, and $11T_2$ have moderate oscillator strengths, which are mainly Rydberg, as seen in Table 3. Though Fernandez et al. attributed these bands to the Rydberg s states and valence antibonding excitations, their result seems to be less reliable in this region, due to the deficiency of the diffuse basis sets.

Nature of the Excited States. Table 3 summarizes the excitation energies, oscillator strengths, and nature of the optically allowed, singlet T_2 excited states, while the results of the singlet A_1, E, and T_1 states are shown in Table 4. All of the excited states calculated here represent the transitions from HOMOs, $6t_2\sigma$ Sn(5p)+H(s) bonding MOs. The SnH_4 homologues CH_4, SiH_4, and GeH_4 show Rydberg-type excitations.[7]

We also calculated the ionized states. The lowest ionized state is the ionization from HOMOs, $6t_2\sigma$ Sn(5p)+H(s) bonding MOs, with a calculated ionization energy of 11.46 eV, and the second lowest state is from $a_1\sigma$, Sn(5s)+H(s) bonding MO, with an energy of 16.47 eV. Our calculated energies agree well with the experimental values of 11.27 and 16.88 eV.[20]

To analyze the Rydberg character of the excited states, we examined the second moment, which is the expectation value of r^2 and reflects the size of the electron-cloud distribution. Generally, Rydberg states have larger second moments than the valence excited states, and those with higher quantum numbers show smaller oscillator strengths and larger second moments. We also examined the ratio of the kinetic and total energies, which is the virial coefficient of a Rydberg electron. We defined the kinetic energy of a Rydberg electron as the difference in kinetic energy between the excited state and the ionized state. The total energy of a Rydberg electron, which is called the term value, is defined similarly. The virial theorem tells us that the ratio of the two energies for a Rydberg electron is equal to unity for a pure Rydberg state.

These two kinds of energies are shown in Figure 3 for each T_2 excited state of SnH_4: we see a trend for convergence to the ionization limit with a small oscillation. The Rydberg s state has a larger kinetic/total energy ratio than the Rydberg p state, as expected from the difference in penetration. The $1T_2$ and $2T_2$ states have a larger kinetic/total energy ratio than other states, which reflects their antibonding natures. Thus, an electron is more likely to stay near the nucleus in these excited

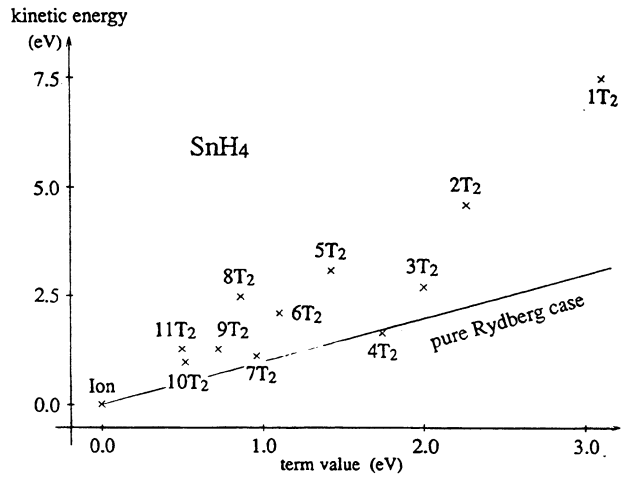

Figure 3. Kinetic energy and total energy of a Rydberg electron in singlet T_2 excited states of SnH_4.

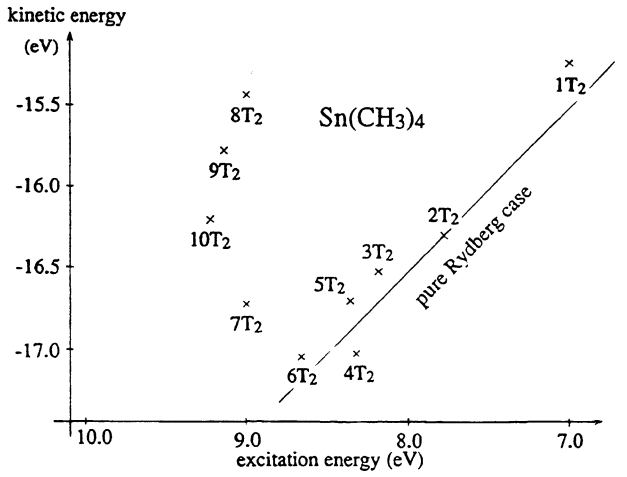

Figure 4. Kinetic energy and total energy of a Rydberg electron in singlet T_2 excited states of $Sn(CH_3)_4$.

states. The $1T_2$ state is Rydberg s mixed with $a_1\sigma^*$, Sn(5s)−H(s) antibonding orbital, while the $2T_2$ state is Rydberg d mixed with $t_2\sigma^*$, Sn(5p)−H(s).

Tables 3 and 4 show the Mulliken population analysis for the calculated excited states. A population analysis is somewhat risky when diffuse basis sets are involved. The large overlap between the diffuse basis functions causes negative, unphysical populations. Therefore, we mainly examined the valence populations.

The Rydberg s states have large populations in the Rydberg s functions on Sn. The Rydberg p and d states show similar trends. In the $1T_2$ state, the Rydberg s functions on hydrogens have relatively large populations, as expected from its $a_1\sigma^*$ antibonding character. These diffuse functions seem to occupy part of the valence atomic orbitals. In the $2T_2$ state, the valence Sn(p) function has the largest population among the calculated T_2 states, which shows its $t_2\sigma^*$ antibonding character. We can understand why the Rydberg 6s and 5d states mix with the antibonding ones. The Rydberg 6s orbital has one more node than 5s in the valence region. On the other hand, the $a_1\sigma^*$ Sn(5s)−H(s) antibonding orbital has a node in the Sn−H bond, like the Rydberg Sn(6s) orbital. Therefore, there must be substantial mixing between these two orbitals. The same explanation can be applied to Sn(5d) and $t_2\sigma^*$ Sn(5p)−H(s). The $1T_1$, 1E, and $1A_1$ states, with excitation energies of 8.27, 8.48, and 8.92 eV, have relatively small second moments and large populations in the valence H(s), as shown in Table 4. The $1T_1$ state also has a large population in the valence Sn(p). This reflects their $t_2\sigma^*$ Sn(5p)−H(s) antibonding character.

Results for $Sn(CH_3)_4$

Ground State. The energies and the nature of the HF valence occupied MOs of $Sn(CH_3)_4$ are shown in Table 2, in which + denotes a bonding combination. The HOMOs $9t_2$ are Sn(5p)+C(2p) bonding MOs. There are many unoccupied MOs with positive orbital energies, as in SnH_4. The Hartree−Fock total energy of $Sn(CH_3)_4$ is −6176.9084 au, and the correlation energy calculated by the SAC method is −0.154 695 au.

Comparison with VUV Spectrum of $Sn(CH_3)_4$. Figure 2 compares our SAC-CI results with the experimental spectrum of $Sn(CH_3)_4$, which shows two broad absorption bands. The dotted peaks show the results of the deconvolution analysis by Fernandez et al.[6] Table 5 gives the details of the calculated T_2 states. The dipole-forbidden transitions are shown in Figure 2 by open circles on the energy axis; details are given in Table 6.

The inset of Figure 2 shows the result of ab initio calculations by Fernandez et al. Similarly to Figure 1 for SnH_4, they gave only two T_2 states in this energy region, while our calculations give a lot of states. In particular, they cannot explain the strongest peak at around 9.0 eV. The reason is clear: they did not include the Rydberg-type basis functions which are of crucial importance for studying the excited states of saturated molecules like $Sn(CH_3)_4$.

The first broad absorption centered at 6.7 eV is assigned to the $1T_2$ state calculated at 7.01 eV. This state is Rydberg 6s mixed with the $a_1\sigma^*$ antibonding orbital, which is the same as that given by Fernandez et al.[6] Its nature and the term value are similar to those of SnH_4, though $Sn(CH_3)_4$ shows no remarkable Jahn−Teller splitting. The Jahn−Teller distortion of the $Sn(CH_3)_4^+$ cation has been studied extensively.[21]

The second broad absorption centered at 8.9 eV is assigned to the $8T_2$ state calculated at 8.98 eV, which is Rydberg 6d mixed with the $t_2\sigma^*$ antibonding orbitals. Many excited states of moderate intensity were also calculated ($3T_2$, $5T_2$, $6T_2$, and $9T_2$). In contrast, Fernandez et al. did not calculate any states in this energy region, due to the deficiency of the diffuse basis function. The $10T_2$ and $11T_2$ states represent the excitations to the Rydberg f-like orbitals, which were represented by the p functions on carbons, since our basis set does not involve any f functions. Some components of the Rydberg f orbital have the same symmetry as the t_1 antibonding orbital in a T_d molecule. On the basis of their small intensities, we tentatively considered them Rydberg f states rather than valence antibonding states. Overall, our calculation agrees well with the experimental spectrum.

Nature of the Excited States. Table 5 summarizes the excitation energies, oscillator strengths, and the nature of the singlet T_2 excited states, and the results for the singlet A_1, E, and T_1 states are shown in Table 6. All of the excited states calculated below the experimental first IP, 9.70 eV,[22] are the transitions from HOMOs, $9t_2\sigma$ Sn(5p)+C(2p) bonding MOs. We reproduced some members of the Rydberg series. To analyze the Rydberg character of the excited states, we calculated the second moment, as shown in Tables 5 and 6. The $8T_2$ state has a relatively small second moment, which implies its antibonding nature. We also examined the ratio of the kinetic/total energy of a Rydberg electron. Since we did not calculate the ionized state, we defined the kinetic energy of a Rydberg electron as the difference in kinetic energy between the excited state and the ground state. This definition differs

TABLE 5: Excitation Energies, Oscillator Strengths, and the Nature of the Singlet T_2 (Dipole-Allowed) Excited States of $Sn(CH_3)_4$

				Mulliken population[a]							
				Sn					C		
state	excitation energy (eV)	oscillator strength ($\times 10^{-2}$)	second moment (au)	val s	val p	Ryd s	Ryd p	Ryd d	val p	Ryd s	nature[b]
XA_1	0.0		851	0.78	0.86	−0.06	−0.40	−0.29	3.32	0.34	ground state, Hartree−Fock
$1T_2$	7.01	27.5	913	0.67	0.71	−0.06	−0.18	0.11	3.15	0.50	Sn(p)+C(p) → Sn(6s), Sn(5s)−C(s)
$2T_2$	7.78	0.50	946	0.74	0.74	−0.01	0.45	−0.01	3.14	0.38	Sn(p)+C(p) → Sn(6p)
$3T_2$	8.19	11.7	992	0.74	0.77	−0.05	−0.30	0.34	3.15	0.31	Sn(p)+C(p) → Sn(5d)
$4T_2$	8.31	1.88	1007	0.75	0.77	0.02	−0.21	1.24	3.15	0.32	Sn(p)+C(p) → Sn(5d)
$5T_2$	8.37	5.80	1138	0.71	0.76	1.24	−0.14	−0.90	3.15	0.36	Sn(p)+C(p) → Sn(7s)
$6T_2$	8.65	4.09	1226	0.74	0.77	0.38	−0.44	−0.44	3.15	0.36	Sn(p)+C(p) → Sn(7p)
$7T_2$	8.97	0.49	1243	0.73	0.75	−0.20	−0.10	0.58	3.15	0.28	Sn(p)+C(p) → Sn(8s)
$8T_2$	8.98	30.2	1031	0.75	0.81	−0.06	−0.04	0.27	3.15	0.30	Sn(p)+C(p) → Sn(6d), Sn(5p)−C(p)
$9T_2$	9.13	13.3	1080	0.76	0.76	−0.16	−0.29	0.65	3.15	0.28	Sn(p)+C(p) → Sn(6d)
$10T_2$	9.17	0.55	1090	0.75	0.77	−0.05	−0.09	0.59	3.15	0.28	Sn(p)+C(p) → Sn(f)

[a] Abbreviations: val and Ryd = valence and Rydberg, respectively. [b] + and − indicate bonding and antibonding combinations.

TABLE 6: Excitation Energies and the Nature of the Singlet A_1, E, and T_1 (Dipole-Forbidden) Excited States of $Sn(CH_3)_4$

			Mulliken population[a]							
			Sn					C		
state	excitation energy (eV)	second moment (au)	val s	val p	Ryd s	Ryd p	Ryd d	val p	Ryd s	nature[b]
XA_1	0.0	851	0.78	0.86	−0.06	−0.40	−0.29	3.32	0.34	ground state, Hartree−Fock
$1A_1$	7.56	941	0.74	0.71	−0.05	0.67	−0.21	3.15	0.44	Sn(p)+C(p) → Sn(6p)
$1T_1$	7.62	930	0.75	0.76	−0.05	0.51	0.05	3.14	0.37	Sn(p)+C(p) → Sn(6p)
1E	7.65	933	0.75	0.72	−0.05	1.22	−0.04	3.14	0.44	Sn(p)+C(p) → Sn(6p)
$2T_1$	8.24	977	0.75	0.80	−0.04	−0.26	1.51	3.15	0.30	Sn(p)+C(p) → Sn(5d)
$2A_1$	8.30	1002	0.75	0.76	−0.04	0.10	0.63	3.14	0.29	Sn(p)+C(p) → Sn(5d)
2E	8.34	1009	0.75	0.77	−0.04	−0.11	1.02	3.15	0.24	Sn(p)+C(p) → Sn(5d)
$3T_1$	8.35	1016	0.75	0.78	−0.04	0.05	0.61	3.15	0.34	Sn(p)+C(p) → Sn(5d)
$4T_1$	8.52	1109	0.75	0.81	−0.03	0.28	0.09	3.15	0.36	Sn(p)+C(p) → Sn(7p)
3E	8.54	1149	0.75	0.78	−0.05	0.40	−0.12	3.14	0.40	Sn(p)+C(p) → Sn(7p)
$3A_1$	8.58	1207	0.75	0.74	−0.05	0.56	−0.21	3.15	0.37	Sn(p)+C(p) → Sn(7p)
$5T_1$	8.78	1146	0.75	0.78	−0.04	0.02	−0.08	3.15	0.26	Sn(p)+C(p) → Sn(5p)−C(p)
4E	8.83	1132	0.75	0.80	−0.05	0.19	0.07	3.15	0.28	Sn(p)+C(p) → Sn(5p)−C(p)
$4A_1$	9.04	1050	0.75	0.83	−0.04	-4×10^{-3}	0.16	3.15	0.34	Sn(p)+C(p) → Sn(5p)−C(p)
$6T_1$	9.14	1200	0.75	0.78	−0.05	0.27	0.38	3.15	0.28	Sn(p)+C(p) → Sn(6d)
$5A_1$	9.17	1215	0.75	0.76	−0.04	0.77	0.14	3.15	0.19	Sn(p)+C(p) → Sn(8p)

[a] Abbreviations: val and Ryd = valence and Rydberg, respectively. [b] + and − indicate bonding and antibonding combinations.

from the previous definition by a constant. The total energy of a Rydberg electron is defined similarly.

These two kinds of energies are shown in Figure 4 for each T_2 state of $Sn(CH_3)_4$. In this case, the $1T_2$ and $8T_2$ states have a larger kinetic energy ratio than other states, which indicates their antibonding character. The $1T_2$ and $8T_2$ states have primarily Rydberg 6s and 6d characters, respectively, mixed with Sn−C antibonding orbitals. The Mulliken population analysis in Table 5 shows that the $1T_2$ state has a relatively large population in the Rydberg s function on carbon, which is similar to the result with SnH_4. Therefore, the mixed antibonding orbital in the $1T_2$ state is $a_1\sigma^*$ Sn(5s)−C(2s). On the other hand, the $8T_2$ state has a relatively large population on the valence Sn(p) function, which reflects its $t_2\sigma^*$ antibonding character. We can understand why the Rydberg 6d orbital, rather than 5d, mixes with the antibonding orbital. The mixed orbital is the Sn(5p)−C(2p) antibonding orbital, which has one additional node due to C(2p). Therefore, Sn(6d) is more suitable than Sn(5d) for mixing with this antibonding orbital. The difference in the VUV spectra between SnH_4 and $Sn(CH_3)_4$ is attributed to the difference in the nodes of these $t_2\sigma^*$ antibonding orbitals. The $5T_1$, 4E, and $4A_1$ states, with excitation energies of 8.78, 8.83, and 9.04 eV, have relatively small second moments and large populations on the valence Sn(p) function, as shown in Table 6, which reflects their $t_2\sigma^*$ Sn(5p)−C(2p) antibonding character.

Summary

We used the SAC/SAC-CI method and large basis sets with many Rydberg-type basis functions to calculate the excited states of SnH_4 and $Sn(CH_3)_4$ up to the first IP. We successfully reproduced the VUV spectra for both excitation energies and intensities. The assignments of the lowest T_2 states agree with earlier works by Fernandez et al. In the higher energy region, where inclusion of enough Rydberg-type basis functions is essentially important, we calculated many states which have been overlooked in the earlier works. We have provided new assignments and clarified the nature of the excited states. The excitations in this energy region are primarily Rydberg. However, some states show a strong mixing with antibonding orbitals and are characterized by smaller second moments and larger oscillator strengths.

The difference in the VUV spectra between SnH_4 and $Sn(CH_3)_4$ can be explained as follows: in SnH_4, the Rydberg Sn(6s) orbital mixes with the $a_1\sigma^*$ Sn(5s)−H(s) antibonding orbital, while the Rydberg Sn(5d) orbital mixes with the $t_2\sigma^*$ Sn(5p)−H(s) orbitals. In $Sn(CH_3)_4$, on the other hand, the Rydberg Sn(6s) orbital mixes with the $a_1\sigma^*$ Sn(5s)−C(2s) orbital, while the Rydberg Sn(6d) orbital mixes with the $t_2\sigma^*$ Sn(5p)−C(2p) orbitals. The mixing with the C(2p) orbital results in an additional node for the Rydberg orbital.

Acknowledgment. We thank Mr. M. Sugimoto and Drs. M. Hada and H. Nakai for their helpful discussions in the course

of this study. The SAC/SAC-CI calculations were partially performed on the HITAC M-680H and S-820 computers at the Institute for Molecular Science. This study was supported in part by a Grant-in-Aid for Scientific Research from the Japanese Ministry of Education, Science and Culture. K.Y. acknowledges a fellowship from the Japan Society for the Promotion of Science.

References and Notes

(1) (a) Osmundsen, J. F.; Abele, C. C.; Eden, J. G. *J. Appl. Phys.* **1985**, *57*, 2921. (b) Hata, N.; Matsuda, A.; Tanaka, K. *J. Appl. Phys.* **1987**, *61*, 3055. (c) Tsuji, M.; Kobarai, K.; Nishimura, Y. *J. Chem. Phys.* **1990**, *93*, 3133. (d) Funsten, H. O.; Boring, J. W.; Johnson, R. E. *J. Appl. Phys.* **1992**, *71*, 1475.

(2) (a) Perrin, J.; Schmitt, J. P. M. *Chem. Phys.* **1982**, *67*, 167. (b) Schmitt, J. P. M.; Gressier, P.; Krishnan, M.; deRosny, G.; Perrin, J. *Chem. Phys.* **1984**, *84*, 281. (c) Börlin, K.; Heinis, T.; Jungen, M. *Chem. Phys.* **1986**, *103*, 93.

(3) (a) Blunden, S. J.; Hobbs, L. A.; Smith, P. J. In *Environmental Chemistry*; Bowen, H. J. M., Ed.; Chemical Society: London, 1984. (b) Brinckman, F. E.; Jackson, J. A.; Blair, W. R.; Olson, G. J.; Iverson, W. P. In *Trace Metal in Sea Water*; Wong, C. S., Ed.; NATO ASI Ser.; Plenum Press: New York, 1982.

(4) (a) Mahan, B. H.; Mandal, R. *J. Chem. Phys.* **1962**, *37*, 207. (b) Ring, M. A.; Beverly, G. D.; Koester, F. H.; Hollandsworth, R. P. *Inorg. Chem.* **1969**, *8*, 2033. (c) Perkins, G. G. A.; Austin, E. R.; Lampe, F. W. *J. Am. Chem. Soc.* **1979**, *101*, 1109.

(5) Fernandez, J.; Lespes, G.; Dargelos, A. *Chem. Phys.* **1986**, *103*, 85.

(6) Fernandez, J.; Lespes, G.; Dargelos, A. *Chem. Phys.* **1986**, *111*, 97.

(7) Robin, M. B. *Higher Excited States of Polyatomic Molecules*; Academic Press: New York, 1974.

(8) (a) Buenker, R. J.; Peyerimhoff, S. D. *Chem. Phys. Lett.* **1975**, *36*, 415. (b) Peyerimhoff, S. D. *Gazz. Chim. Ital.* **1978**, *108*, 411.

(9) Nakatsuji, H.; Hirao, K. *J. Chem. Phys.* **1978**, *68*, 2053.

(10) Nakatsuji, H. *Chem. Phys. Lett.* **1978**, *59*, 362; **1979**, *67*, 329, 334.

(11) (a) Nakatsuji, H. *Acta Chim. Hung.* **1992**, *129*, 719. (b) Nakatsuji, H. *J. Chem. Phys.* **1984**, *80*, 3703. (c) Nakatsuji, H.; Kitao, O.; Yonezawa, T. *Ibid.* **1985**, *83*, 723. (d) Nakatsuji, H.; Kitao, O. *Ibid.* **1987**, *87*, 1169. (e) Kitao, O.; Nakatsuji, H. *Chem. Phys. Lett.* **1988**, *143*, 528.

(12) (a) Yasuda, K.; Nakatsuji, H. *J. Chem. Phys.* **1993**, *99*, 1945. (b) Nakatsuji, H.; Ehara, M.; Palmer, M. H.; Guest, M. *J. Chem. Phys.* **1992**, *97*, 2561. (c) Nakai, H.; Ohmori, Y.; Nakatsuji, H. *J. Chem. Phys.* **1991**, *95*, 8287. (d) Nakatsuji, H.; Saito, S. *Int. J. Quantum Chem.* **1991**, *39*, 93. (e) Nakatsuji, H.; Saito, S. *J. Chem. Phys.* **1990**, *93*, 1865. (f) Nakatsuji, H.; Sugimoto, M.; Saito, S. *Inorg. Chem.* **1990**, *29*, 3095. (g) Jitsuhiro, S.; Nakai, H.; Hada, M.; Nakatsuji, H. *J. Chem. Phys.* **1994**, *101*, 1029.

(13) (a) Callomon, J. H.; Hirota, E.; Kuchitsu, K.; Lafferty, W. J.; Maki, A. G.; Pote, C. S. *Landolt-Bornstein New Series Supplement II/7*; Springer: Berlin, 1987. (b) Callomon, J. H.; Hirota, E.; Iijima, T.; Kuchitsu, K.; Lafferty, W. J. *Landolt-Bornstein New Series Supplement II/15*; Springer: Berlin, 1987.

(14) Huzinaga, S.; Andzelm, J.; Klobukowski, M.; Radzio-Andzelm, E.; Sakai, Y.; Tatewaki, H. *Gaussian Basis Sets for Molecular Calculations*; Elsevier: Amsterdam, 1984.

(15) Dunning, T. H., Jr. *J. Chem. Phys.* **1970**, *53*, 2823.

(16) Jungen, M. *J. Chem. Phys.* **1981**, *74*, 750.

(17) Dunning, T. H., Jr.; Hay, P. J. In *Methods of Electronic Structure Theory, Gaussian Basis Sets for Molecular Calculation*; Schaefer, H. F., Ed.; Plenum Press: New York, 1977.

(18) (a) Nakatsuji, H. Program system for SAC and SAC-CI calculations, Program Library No. 146 (Y4/SAC), Data Processing Center of Kyoto University, 1985. (b) Nakatsuji, H. Program Library SAC85 (No. 1396), Computer Center of the Institute for Molecular Science, Okazaki, 1986.

(19) Nakatsuji, H. *Chem. Phys.* **1983**, *75*, 425.

(20) (a) Potts, A. W.; Price, W. C. *Proc. R. Soc. London* **1972**, *A326*, 165. (b) Dewer, M. J. S.; Grady, G. L.; Kuhn, D. R. *Organometallics* **1985**, *4*, 1041. (c) Fernandez, J.; Arriau, J.; Dargelos, A. *Chem. Phys.* **1985**, *94*, 397. (d) Caballol, R.; Catala, J. A.; Problet, J. M. *Chem. Phys. Lett.* **1986**, *130*, 278. (e) Fernandez, J.; Teichteil, C.; Dargelos, A. *Chem. Phys.* **1987**, *114*, 201. (f) Kudo, T.; Nagase, S. *Chem. Phys. Lett.* **1989**, *156*, 289.

(21) (a) Symons, M. C. R. *J. Chem. Soc., Chem. Commun.* **1982**, 869. (b) Hasegawa, A.; Kaminaka, S.; Wakabayashi, T.; Hayashi, M.; Symons, M. C. R. *J. Chem. Soc., Chem. Commun.* **1983**, 1199. (c) Walther, B. W.; Williams, F.; Lau, W.; Kochi, J. K. *Organometallics* **1983**, *2*, 688. (d) Bonazzola, L.; Michaut, J. P.; Roncin, J. *New J. Chem.* **1992**, *16*, 489.

(22) (a) Evans, S.; Green, J. C.; Joachim, P. J.; Orchard, A. F.; Turner, D. W.; Maier, J. P. *J. Chem. Soc., Faraday Trans. 2* **1972**, *68*, 905. (b) Bancroft, G. M.; Pellach, E.; Tse, J. S. *Inorg. Chem.* **1982**, *21*, 2950. (c) Novak, I.; Benson, J. M.; Svensson, A.; Potts, A. W. *Chem. Phys. Lett.* **1987**, *135*, 471.

JP9500955